

## **Circulating HDL levels control hypothalamic astrogliosis via ApoA-I**

Anna Götz<sup>1,2</sup>, Maarit Lehti<sup>3</sup>, Elizabeth Donelan<sup>4</sup>, Cynthia Striase<sup>5</sup>, Sebastian Cucuruz<sup>5</sup>, Stephan Sachs<sup>5</sup>, Chun-Xia Yi<sup>6</sup>, Stephen C. Woods<sup>4</sup>, Samuel D. Wright<sup>7</sup>, Matthias H. Tschöp<sup>1,8</sup>, Yuanqing Gao<sup>9#</sup>, Susanna M. Hofmann<sup>5,8,10\*</sup>

<sup>1</sup> Institute for Diabetes and Obesity, Helmholtz Zentrum München, German Research Center for Environmental Health (GmbH), Ingolstaedter Landstr. 1, 85764 Neuherberg, Germany.

<sup>2</sup> Department of Internal Medicine I, University Hospital RWTH Aachen, Pauwelsstraße 30, 52074 Aachen, Germany

<sup>3</sup> LIKES Research Center for Sport and Health Sciences, Viitaniementie 15a, 40720 Jyväskylä, Finland

<sup>4</sup> Metabolic Disease Institute, Department of Internal Medicine, University of Cincinnati, 2180 E. Galbraith Road, Cincinnati, OH 45215, USA

<sup>5</sup> Institute for Diabetes and Regeneration Research, Helmholtz Zentrum München, German Research Center for Environmental Health (GmbH), Ingolstaedter Landstr. 1, 85764 Neuherberg, Germany.

<sup>6</sup> Department of Endocrinology and Metabolism, Academic Medical Center, University of Amsterdam, The Netherlands

<sup>7</sup> CSL Behring, 120 First Avenue, King of Prussia, PA, USA

<sup>8</sup> German Center for Diabetes Research (DZD) München-Neuherberg Germany

<sup>9</sup> Nanjing Medical University, College of Pharmacy, Nanjing, China.

<sup>10</sup> Medizinische Klinik und Poliklinik IV, Klinikum der Ludwig Maximilian Universität, Ziemssenstr. 1, 80336 Munich, Germany

\* To whom correspondence should be addressed: Susanna Hofmann, Institute for Diabetes and Regeneration Research, German Research Center for Environmental Health (GmbH), Ingolstaedter Landstr. 1, 85764 Neuherberg, Germany, Phone: ++49-89-3187-2112 Fax: +49-89-318-2008 ; Email:

[susanna.hofmann@helmholtz-muenchen.de](mailto:susanna.hofmann@helmholtz-muenchen.de)

# Co-corresponding author: Yuanqing Gao, Nanjing Medical University, college of Pharmacy, Nanjing, China,  
Email: [yuanqinggao@njmu.edu.cn](mailto:yuanqinggao@njmu.edu.cn)

Running title: Apolipoprotein AI deficiency enhances hypothalamic inflammation and obesity

Abbreviations: ATP5b = ATP synthase subunit beta; ApoA-I = apolipoprotein I; ARC = arcuate nucleus; ATP = adenosine triphosphate; Cyt1 = cytochrome C1; 2DG= 2-deoxy-glucose; ETC = electron transfer chain; ECAR = extracellular acidification rate; FCCP = carbonyl cyanide-4-(trifluoromethoxy)phenylhydrazone; GFAP = glial fibrillary acidic protein; HDL = high density lipoprotein; Iba-1 = ionized calcium binding adaptor molecule 1; Mit2 = mitofusin 2; OCR = oxygen consumption rate; Opa1 = optic atrophy 1; OXPHOS = oxidative phosphorylation; PGC1- $\alpha$  = peroxisome proliferator-activated receptor c coactivator 1 alpha

## **ABSTRACT**

Meta-inflammation of hypothalamic areas governing energy homeostasis has recently emerged as a process of potential pathophysiological relevance for the development of obesity and its metabolic sequelae. The current model suggests that diet-induced neuronal injury triggers microgliosis and astrocytosis, conditions which ultimately may induce functional impairment of hypothalamic circuits governing feeding behavior, systemic metabolism and body weight. Epidemiological data indicate that low circulating HDL levels, besides conveying cardiovascular risk, also correlate strongly with obesity. We simulated that condition by using a genetic loss of function mouse model (apoA-I<sup>-/-</sup>) with markedly reduced HDL levels to investigate whether HDL may directly modulate hypothalamic inflammation. Astroglia was significantly enhanced in the hypothalami of apoA-I<sup>-/-</sup> compared to apoA-I<sup>+/+</sup> mice and was associated with compromised mitochondrial function. ApoA-I<sup>-/-</sup> mice exhibited key components of metabolic disease like increased fat mass, fasting glucose levels, hepatic triglyceride content and hepatic glucose output compared to apoA-I<sup>+/+</sup> controls. Administration of rHDL (CSL-111) normalized hypothalamic inflammation and mitochondrial function markers in apoA-I<sup>-/-</sup> mice. Treatment of primary astrocytes with apoA-I resulted in enhanced mitochondrial activity, implying that circulating HDL levels are likely important for astrocyte function. HDL-based therapies may consequently avert reactive gliosis in hypothalamic astrocytes by improving mitochondrial bioenergetics and thereby offering potential treatment and prevention for obesity and metabolic disease.

## **Supplementary keywords**

mitochondria, inflammation, HDL, apoA-I, metabolism, dyslipidemia, adipose tissue, hypothalamus, astrocytes

## INTRODUCTION

Obesity is associated with a state of moderate but chronic inflammation that is characterized by increased tissue-specific levels, as well as circulating levels, of interleukins and cytokines, a condition that is thought to participate in the development of many obesity-associated comorbidities by inducing cellular dysfunction (1). Emerging evidence indicates that chronic consumption of excess calories induces inflammation in the arcuate nucleus (ARC) of the hypothalamus, a brain area important for the regulation of food intake and energy expenditure (2). This process is considered an early and determining factor for the onset of obesity since it occurs prior to body weight gain and participates in the development and progression of metabolic disorders including obesity, diabetes and cardiovascular disease. Mitochondrial activity, which is critical for proper functioning of the central nervous system, is compromised in inflammatory states, and there are documented molecular links among inflammation, impaired insulin signaling and mitochondrial dysfunction in neurodegenerative diseases and diabetes (3). Novel therapeutic strategies may therefore be developed to target this impairment.

Within the hypothalamus, glial cells are key regulators of parenchymal homeostasis and neuronal communication. Glial cells become activated during periods of excess caloric intake, causing them to initiate inflammatory processes known collectively as reactive gliosis. As this occurs, the two main classes of glial cells, astrocytes and microglia, are converted to an activated pro-inflammatory phenotype characterized by cellular hypertrophy and proliferation, increased expression of intermediate filaments and secretion of inflammatory interleukins and cytokines (2). Glial cells can also be activated directly by several pro-inflammatory factors or cytokines, including the metabolic hormone leptin, which stimulate the production of IL1 $\beta$ , TNF $\alpha$  and IL 6 within the glial cells (4). Activated microglia and astrocytes continue to accumulate in the hypothalamus over months of excess caloric intake, such that hypothalamic inflammation becomes persistent, potentially leading to neuronal dysfunction and thus to a chronic impairment of energy homeostasis (5).

Epidemiological studies have confirmed a strong association between fat intake, plasma cholesterol levels, obesity and cardiovascular disease mortality (6, 7). One key independent predictor for cardiovascular disease as

well as for Alzheimer's dementia is a low level of high-density lipoprotein (HDL) particles and their major protein constituent, apolipoprotein A-I (apoA-I) (8-10). Low circulating HDL and apoA-I are also a hallmark of obesity in association with insulin-resistance, a pathological precondition associated with type-2 diabetes mellitus (T2D) (11). HDLs have atheroprotective functions that are independent of their well-known role in lipid transport (12). In particular, HDLs directly mediate anti-inflammatory reprogramming of immune cells (13), promoting cerebrovascular health (10) and maintaining mitochondrial function (for review see 14), activities that may prevent and/or ameliorate metabolic disease. However, it is not known whether circulating HDLs exert an independent effect on the development of obesity and metabolic dysfunction. We therefore investigated the role of genetically reduced HDL levels in the development of hypothalamic inflammation and mitochondrial dysfunction. Using a genetic loss of function mouse model ( $\text{apoA-I}^{-/-}$ ), we report for the first time that low circulating HDL levels promote specifically astrocyte activation and induce mitochondrial dysfunction within the hypothalamic astrocytes that is associated with enhanced adiposity and impaired glucose homeostasis. Treatment of primary astrocytes with apoA-I results in enhanced mitochondrial bioenergetics of primary astrocytes and administration of rHDL (CSL-111) in  $\text{apoA-I}^{-/-}$  mice reverses hypothalamic inflammation by normalizing mitochondrial function markers, suggesting that HDL-based therapies may avert astroglial dysfunction and thus offer a new approach for potential treatment and prevention of obesity and metabolic disease.

## **MATERIALS AND METHODS**

### **Animals**

For phenotyping studies, apolipoprotein A-I deficient (apoA-I<sup>-/-</sup>) male mice on the C57/BL/6J background (Jackson Laboratories, Bar Harbor, ME) were bred with female wild type mice in our animal facilities. Age-matched male apoA-I<sup>-/-</sup> mice and their wildtype male littermates (apoA-I<sup>+/+</sup>) mice (n = 10-14/group) were six months of age at the initiation of the study.

For pharmacological studies, reconstituted human HDL (CSL-111) was provided by CSL Behring AG (Bern, Switzerland) and prepared from human plasma as previously described (15). The preparation was supplied as a lyophilized powder that upon reconstitution with sterile water rendered a solution containing 19.5g/L protein. The molar ratio protein–phospholipid was 1:155. Seven-month old apolipoprotein A-I deficient (apoA-I<sup>-/-</sup>) male mice and wt mice (n=6/group) were randomized according to body weight and body composition. Mice were treated daily via intraperitoneal injections of CSL-111 (150mg/kg) for seven days during light cycle. Vehicle mice received an equivalent volume of 0.9% saline.

All mice were housed in a pathogen-free environment on a 12:12-h light-dark cycle at 22°C with free access to food and water. Mice were fed a regular chow diet (5058 PicoLab Mouse Diet 20, LabDiet, Richmond, IN). Body fat mass was measured in conscious mice using 1H magnetic resonance spectroscopy (EchoMRI-100; Echo- medical Systems). All rodent studies were approved by and performed according to the guidelines of the Institutional Animal Care and Use Committee at the University of Cincinnati and the Helmholtz Center Munich.

### **Biochemical Assays**

Animals were fasted for 6 h prior to blood collection from the tail vein. Plasma cholesterol levels were determined using the Infinity Cholesterol Kit (Thermo Scientific Inc, Rockford, IL) as described (16). An intraperitoneal pyruvate tolerance test was conducted by injection of sodium pyruvate (2g/kg, Sigma, St. Louis, MO, USA) in 0.9% wt/vol NaCl as described previously (17). Tail blood glucose levels [mg/dl] were measured with glucometer TheraSense Freestyle (Abbott Diabetes Care, Inc., Alameda, CA) before (0 min) and at 15, 30, 45, 60 and 120 min after injection. Samples were analyzed individually except for lipoprotein separation, for

which pooled samples were subjected to fast-performance liquid chromatography (FPLC) as described previously (16).

Brain cortex and liver lipid content of ad libitum-fed mice was assessed by extraction as described (16). Briefly, 20 mg of snap-frozen brain cortex and 50 mg of snap-frozen liver was homogenized with 1 ml chloroform. Lipids were extracted by overnight shaking at room temperature. For phase separation, 700  $\mu$ l of ddH<sub>2</sub>O were added, samples were centrifuged at 2000 rpm for 20 min at 4°C and the organic layer was collected. For the second extraction, 700  $\mu$ l chloroform/methanol (2:1 vol/vol) was added to the remaining homogenate and lipid extraction, and phase separation and organic-layer collection were performed as described above. 15  $\mu$ l of both extractions were then transferred to glass tubes, evaporated and measured with Infinity Cholesterol and Triglyceride Kit (Thermo Scientific Inc, Rockford, IL).

Brain cortex tissue was snap frozen for determination of citrate synthase activity by a colorimetric assay kit (K318-100, Biovision, Germany). Assay was carried out according to the manufacture's instruction. Briefly, frozen tissues were homogenized with assay buffer and incubated with substrate mix. Enzyme activity was calculated from standard curve. Protein level was determined by a Pierce BCA Protein Assay kit (Thermo Fisher, Germany). Citrate synthase activity was normalized to protein content.

### **Immunohistochemistry and quantitative analysis**

At the termination of the study, mice were decapitated and brains were removed and immerse-fixed in 4% paraformaldehyde at 4 °C for 24 h. Brains were then equilibrated 48 h with 30% sucrose in 0.1 M Tris-buffered saline (TBS, pH 7.2). Immunohistochemistry and quantitative analysis for ionized calcium binding adaptor molecule 1 (iba1) and glial fibrillary acidic protein (GFAP) were performed on coronal brain sections (30  $\mu$ m) throughout the hypothalamus as described previously (18). Briefly, after rinsing in 0.1 M TBS, whole-brain sections were incubated with rabbit anti-iba1 primary antibody (Synaptic System, Goettingen, Germany) at 1:1000 dilution or rabbit anti-GFAP primary antibody (Dako, Carpinteria, CA, USA) at 1:1000 dilution overnight at 4 °C. Sections were then rinsed and incubated with biotinylated secondary antibody (horse anti-rabbit IgG, Vector, CA, USA) for 1 h; subsequently, sections were rinsed and incubated in avidin–biotin complex (ABC, Vector, CA, USA) for 1 h. The reaction product was visualized by incubation in 1%

diaminobenzidine with 0.01% hydrogen peroxide for 1-10 min. Sections were mounted on gelatin-coated glass slides, dried, dehydrated in graded ethanol series, cleared in xylene, and cover-slipped for observation by light microscopy. All quantitative analyses were performed under blinded conditions and confirmed by at least two independent researchers. For each mouse, two to three sections in the middle portion of the arcuate nuclei (ARC) within the mediobasal hypothalamus were selected and images were captured by a computerized image analysis system consisting of an Axioskop color video camera (Carl Zeiss International, Thornwood, NY, USA). Both sides of the ARC were manually outlined with an area of 0.04 mm<sup>2</sup> on each side. Immuno-reactive cells were manually counted throughout the ARC, and expressed as number of cells per mm<sup>2</sup>. The average from each mouse was then calculated and expressed as the mean ± SEM from each group.

### **Real-time PCR**

Mice were euthanized by CO<sub>2</sub>. Brains were subsequently harvested and hypothalami were immediately isolated and stored in liquid nitrogen. At a later time point, RNA was isolated by RNeasy Lipid Tissue Mini Kit (Qiagen, Hilden, Germany). After reverse transcription (QuantiTech reverse transcription kit, Qiagen, Hilden, Germany), gene expression was analyzed by real-time PCR (ABI Taqman 7900, Life technologies GmbH, Darmstadt, Germany) using the company's reaction system and probes.

### **Cell Culture**

Hypothalami were isolated from 2-d-old male C57/BL/6J mice and triturated in MEM (Life Technologies, Darmstadt, Germany) containing 1% penicillin-streptomycin, 10% fetal calf serum (FCS; Life Technologies) and 5.5 mM glucose. Astrocyte isolation was performed as described previously (19). The cell suspension was centrifuged for 7 min at 1000 rpm and the pellet was re-suspended and seeded in a 175-cm<sup>3</sup> cell culture flask. Cells were incubated at 37°C and 5% CO<sub>2</sub> for 9 d with a regular medium change every 3 d. Prior to detachment, the flasks were placed in a 37°C shaking incubator at 280 rpm overnight. The cells were then washed and incubated for 2 min at 37°C with a 0.05% trypsin/EDTA solution (Biochrom AG, Berlin, Germany). Trypsinization was blocked with MEM + 10% FCS + 1% antibiotics. After centrifugation for 5 min at 1000 rpm,

supernatant was discharged and the cell pellet was re-suspended in MEM + 10% FCS + 1% antibiotics and seeded in the XF24 plate with 80,000 cells per well (Seahorse Bioscience, North Billerica, MA, USA).

### **Mitochondrial function analysis**

24 h after seeding, the medium was removed and primary astrocytes were washed with PBS before overnight incubation with MEM medium containing 20 µg/ml apoA-I (EMD Chemicals, Inc. San Diego, CA, USA) or 20 µg/ml BSA (Sigma-Aldrich, St. Louis, MO, USA) in quintuplicates as reported (20). The next morning, cells were washed with PBS and incubated with XF assay medium containing 5.5 mM glucose for 1 h in a 37°C air incubator. The XF24 plate was then transferred to a temperature-controlled (37°C) Seahorse (extracellular flux) analyzer (Seahorse Bioscience, North Billerica, MA, USA) and subjected to an equilibration period.

Respirometry analysis was performed as described previously (21). Briefly, one assay cycle consisted of a 1-min mix, 2-min wait, and 3-min measurement period. After 4 basal assay cycles, oligomycin (20 µg/ml) was added by automatic pneumatic injection to inhibit ATP synthase for the determination of the proportion of respiration used to drive ATP synthesis for 3 additional cycles. Subsequently, carbonyl cyanide-4-(trifluoromethoxy)-phenylhydrazone (FCCP; 10 µM) was added the same way to determine maximal respiration in mitochondria by uncoupling ATP synthesis from electron transport for another 3 assay cycles. Finally, rotenone (25 µM) plus antimycin A (25 µM) was added to determine the non-mitochondrial respiratory rate in the next 3 assay cycles, which was then subtracted from all other rates. Oxygen consumption rate (OCR) traces and a scheme about the different modules that we analyzed are depicted in Fig. 3. Coupling efficiency was calculated as the oligomycin-sensitive fraction of mitochondrial respiratory activity. ATP production from oxidative phosphorylation (OXPHOS) was calculated using a phosphate/oxygen (P/O) ratio of 2.3 (22). For analysis of extracellular acidification rates (ECARs) derived from glycolysis, measurements were ended by addition of 2-deoxy-glucose (2DG; 100 mM). ECAR traces and the different modules that we analyzed are depicted in Fig. 4. ECARs were converted into proton production rates (PPRs) by taking into account the buffer capacity. 2DG-sensitive PPR estimates ATP production from glycolysis with a 1:1 ratio. To normalize respirometry readings to cell number per well, cells were stained with crystal violet after the flux experiment in the Seahorse XF Analyzer. Briefly, cells were fixed with 4% paraformaldehyde 30 min at room temperature. After washing 3 times with PBS, 200

$\mu\text{l}$  of 0.1% crystal violet was added into each well and incubated for 10 min. After incubation time, crystal violet was removed and the plate was rinsed with distilled water. When the plate was completely dry, 500  $\mu\text{l}$  of 10% acetic acid was added into each well. Absorbance was read at 590 nm.

### **Statistical analysis**

Quantitative data are presented as mean  $\pm$  SEM. Values were analyzed for statistically significant differences applying two-tailed, unpaired t tests for comparisons between untreated apoA-I<sup>+/+</sup> and apoA-I<sup>-/-</sup> mice and one-way or two-way Anova tests for CSL treatment comparisons between apoA-I<sup>+/+</sup> and apoA-I<sup>-/-</sup> mice as recommended by the GraphPad Prism for optimal analysis. Data homogeneity was analyzed by Bartlett's test and F test, accordingly.  $P < 0.05$  was considered significant (GraphPad Prism, GraphPad Software, La Jolla, CA, USA; SigmaStat, Systat Software, San Jose, CA, USA).

## **RESULTS**

### **Mice with markedly reduced circulating HDLs exhibit enhanced astrogliosis associated with increased IL-6 expression in the ARC.**

To determine whether circulating HDL levels modulate hypothalamic inflammation, we used a genetic loss of function mouse model for apoA-I (apoA-I<sup>-/-</sup>), the main protein component of HDL. As expected, fast-protein liquid chromatography (FPLC) analysis of apolipoprotein profiles revealed a severely reduced circulating HDL **cholesterol** concentration in apoA-I<sup>-/-</sup> mice compared with wt littermates (apoA-I<sup>+/+</sup>, Figure 1A and B). We found that in the absence of apoA-I, mRNA levels of the inflammatory interleukin 6 (IL-6) were significantly increased in the hypothalamus (Fig. 1C). Glial fibrillary acidic protein (GFAP) is an intermediate filament protein that reliably identifies reactive astrocytes in association with cell process expansion (23, 24). Using immuno-histochemical staining of brain sections for GFAP, we found that astrocytic gliosis is markedly increased specifically in the ARC of apoA-I<sup>-/-</sup> compared to apoA-I<sup>+/+</sup> mice (Fig. 1D). Consistent with increased reactive astrogliosis, we also found that the GFAP-labeled cells were enlarged in size, and had more extensive processes, thus exhibiting the typical pro-inflammatory morphology. In parallel we determined whether ARC microglial cells were activated by immunohistochemistry using the well-established macrophage/microglia-

specific marker calcium-binding protein allograft inflammatory factor 1 (iba1) (25). Iba1 is specifically expressed in activated microglia and is thus regarded as a specific surrogate parameter for microgliosis. It has been commonly used to detect and compare activated microglia in numerous species (26). Our quantitative analysis of brain sections revealed no differences in microglial activation in the ARC between the two genotypes (Fig. 1E). As an additional sign of microglial activation, iba1 positive cells display the typical pro-inflammatory morphology of enlarged cell bodies and thickened processes. Herein, we observed no difference in morphology of microglia in the hypothalami of apoA-I<sup>-/-</sup> compared to apoA-I<sup>+/+</sup> mice. In other regions of the brain, including the hippocampus or the cortex, we did not observe differences in astroglial and microglial activation (Supplemental figure S1A and B). In conclusion, our results indicate that circulating HDLs associate with reactive astrogliosis in the ARC, an area known to play a pivotal role in the regulation of energy balance.

#### **Low circulating HDL levels are associated with increased adiposity, hepatic steatosis and impaired glucose homeostasis in mice fed a low-fat diet.**

To understand whether the increased reactive astrogliosis observed in apoA-I<sup>-/-</sup> mice is associated with early markers of metabolic dysfunction, we determined body composition and circulating glucose levels in apoA-I<sup>-/-</sup> and apoA-I<sup>+/+</sup> mice. Although apoA-I<sup>-/-</sup> mice had similar body weights as apoA-I<sup>+/+</sup> mice when fed a regular chow diet, we confirmed previous results by us and others showing that absence of apoA-I in mice results in increased fat mass (19, 27) (Fig. 2A and B). Hepatic triglyceride content was also markedly increased in apoA-I<sup>-/-</sup> compared to apoA-I<sup>+/+</sup> mice (Fig. 2C), indicating that the excess body fat mass in apoA-I<sup>-/-</sup> mice results in part from an increased triglyceride accumulation within the liver. We next asked whether the hepatic steatosis in apoA-I<sup>-/-</sup> mice is associated with impaired hepatic glucose homeostasis. As depicted in Figure 2D, fasting glucose levels were significantly higher in apoA-I<sup>-/-</sup> compared to apoA-I<sup>+/+</sup> mice, implying deterioration of hepatic glucose metabolism. Consistent with the latter, glucose measurements during a pyruvate-tolerance test (PTT) also revealed an enhanced hepatic glucose output in apoA-I<sup>-/-</sup> mice compared to their apoA-I<sup>+/+</sup> littermates (Fig. 2E). These findings suggest that apoA-I deficiency contributes to impaired hepatic lipid and glucose homeostasis.

### **ApoA-I directly enhances cellular respiration by increasing mitochondrial fluxes in primary astrocytes.**

To determine whether HDL and apoA-I have a direct effect on cellular bioenergetics of primary astrocytes, we measured oxygen consumption rate using a Seahorse XF24 extracellular flux analyzer. For the analysis of the oxygen-consuming processes, we sequentially added inhibitors of the mitochondrial transport chain. Figure 3A depicts the time-lapse measurements of oxygen consumption rates (OCR) in absolute values, which can be divided into distinct modules of oxygen consumption, mitochondrial and cellular processes (Fig. 3B). Our analysis revealed that cellular respiration was increased significantly in primary astrocytes upon incubation with apoA-I relative to astrocytes incubated with BSA (Fig. 3A and C), implying enhanced mitochondrial activity in cells treated with apoA-I. To further dissect whether this increase in cellular respiration is due to increases in mitochondrial and/or non-mitochondrial respiration, we used rotenone (complex I inhibitor) and antimycin A (complex III inhibitor) at the end of the experiment to completely inhibit mitochondrial fluxes (Fig. 3B). As depicted in Figure 3A and 3C, basal mitochondrial respiration was increased in astrocytes treated with apoA-I compared to BSA-treated cells, suggesting that apoA-I induces a higher ATP turnover and demand. Using the ATP synthase inhibitor oligomycin, we determined that both ATP-linked respiration and proton leak are higher in apoA-I treated cells relative to cells treated with BSA (Fig. 3D). Using the protonophore FCCP for the induction of maximal substrate oxidation we further determined that the maximal ATP output which is controlled by substrate oxidation capacity is not significantly increased in apoA-I-treated astrocytes compared to BSA-treated cells (Fig. 3E). Our analysis of spare respiratory capacity determined by subtracting basal respiration from FCCP-induced respiration also revealed no differences between the cells treated with apoA-I or BSA (Fig. 3E). Mitochondrial efficiency, also termed coupling efficiency, was similar between astrocytes treated with apoA-I and with BSA. Taken together, the higher cellular respiration of astrocytes treated with apoA-I can be attributed to apoA-I-enhanced mitochondrial respiration.

### **ApoA-I reduces maximal glycolytic capacity in primary astrocytes.**

To determine whether apoA-I also induces changes in cytoplasmatic glycolysis, the ATP source complementary to mitochondria, we compared extracellular acidification rates (ECAR) in primary astrocytes incubated with

apoA-I or BSA simultaneously to OCR (Fig. 4A). As occurred with OCR, we characterized glycolysis in more detail with the use of specific inhibitors. Non-glycolytic acidification was determined by adding 2-deoxyglucose (2DG), an inhibitor of glycolysis (Fig. 4B). Astrocytes treated with apoA-I had lower cellular acidification values than BSA-treated astrocytes (Fig. 4C). While non-glycolytic acidification rates were comparable between astrocytes treated with apoA-I or BSA, basal glycolytic rates were lower in apoA-I-treated astrocytes (Fig. 4C). The difference in basal glycolytic ECARs of astrocytes treated with apoA-I, as compared with astrocytes treated with BSA, indicates reduced glycolytic ATP production in astrocytes treated with apoA-I. Consistent with the latter, we detected a marked decrease in glycolytic activity when we induced maximal glycolytic rates by inhibiting mitochondrial ATP production with oligomycin (Fig. 4D).

#### **ApoA-I increases the ATP demand fueled by oxidative phosphorylation.**

To better characterize ATP homeostasis in astrocytes treated with apoA-I, we determined ATP production by oxidative phosphorylation within the mitochondria and ATP production by glycolysis within the cytoplasm. Our calculation (described in the material and method section) of the flux data indicates a higher mitochondrial ATP output (Fig. 4E) and a lower glycolytic ATP production (Fig. 4F) in apoA-I treated astrocytes as compared with BSA-treated astrocytes, resulting in a slightly higher, but not significant total ATP turnover in apoA-I-treated cells (Fig. 4G). Calculating the proportions of ATP production from oxidative phosphorylation and glycolysis demonstrated that regardless of treatment, astrocytes utilized mainly oxidative phosphorylation processes to fuel their demand for ATP (Fig. 4H). ApoA-I treatment significantly increases the percentage of mitochondrial ATP production contributing to total ATP production in primary astrocytes.

#### **CSL-111 treatment normalizes hypothalamic inflammation and mitochondrial function markers in chow-fed apoA-I<sup>-/-</sup> mice.**

To test the effect of reconstituted HDL on hypothalamic inflammation, groups of 7 months old male apoA-I<sup>-/-</sup> and apoA-I<sup>+/+</sup> C57BL/6J mice were randomized according to body weight and body composition and treated

once daily via intraperitoneal injection of CSL-111 (150mg/kg) or an equivalent volume of saline (vehicle group) for seven consecutive days. In line with our previous findings analysis of circulating cholesterol levels and apolipoprotein profiles revealed a severely reduced circulating HDL particle concentration in apoA-I<sup>-/-</sup> compared to apoA-I<sup>+/+</sup> mice which completely normalized after a week of CSL-111 treatment (Fig. 5A,B). Confirming our previous results (Fig. 1C and 1D), deficiency in apoA-I enhances hypothalamic mRNA levels of IL 6 and the astrocyte specific marker GFAP, while not modifying levels of the microglial specific marker iba1 (Fig. 5C). Administration of CSL-111 for seven days normalizes these hypothalamic inflammation markers in apoA-I<sup>-/-</sup> mice fed a chow diet (Fig. 5C).

Citrate synthase is an enzyme exclusively present in the mitochondrial matrix and thus a quantitative marker for the presence of intact mitochondria. Our quantitative analysis of citrate synthase activity revealed significantly increased levels in the CNS of CSL-111 treated apoA-I<sup>-/-</sup> mice (Fig. 5D), thus revealing enhanced mitochondrial density after treatment with CSL-111. Mitochondrial energy-transducing capacity is essential for maintenance of cellular function and impaired mitochondrial energy metabolism is a hallmark of different inflammatory diseases (3). As a next step we determined whether CSL-111 treatment is also affecting different mitochondrial markers connected to mitochondrial biogenesis, fusion and oxidative phosphorylation. We found that the mRNA levels of Pgc1 $\alpha$  (master regulator of mitochondrial biogenesis), ATP synthase subunit beta (Atp5b) and cytochrome C1 (Cyc1) (both enzymes involved in oxidative phosphorylation), mitofusin 2 (Mit2, one key enzyme involved in mitochondrial fusion) and optic atrophy 1 (Opa1, mitofusion regulatory gene) were all increased in apoA-I<sup>-/-</sup> mice compared to apoA-I<sup>+/+</sup> mice and that CSL-111 normalized all these markers in apoA-I<sup>-/-</sup> mice (Fig.5E).

CSL-111 treatment reduced fat mass in both apoA-I<sup>+/+</sup> and apoA-I<sup>-/-</sup> mice (Fig. 5F). However, different tissues of apoA-I<sup>-/-</sup> and apoA-I<sup>+/+</sup> mice were affected by this decrease in body fat. In apoA-I<sup>+/+</sup> mice the reduction was mainly visible in visceral fat (Fig. 5G), while in apoA-I<sup>-/-</sup> mice mainly in the liver (Fig. 5H and I) and the brain (Fig. 5J and K). CSL-111 treatment further seemed to normalize lean mass increase in apoA-I<sup>-/-</sup> mice (Fig. 5F). We further observed increased amounts of cholesterol and triglycerides in the brains of apoA-I<sup>-/-</sup> mice (Fig. 5J) compared to apoA-I<sup>+/+</sup> mice. Treatment with CSL-111 normalized both in apoA-I<sup>-/-</sup> mice without affecting lipid levels in the brains of apoA-I<sup>+/+</sup> mice (Fig. 5J, hatched bars). Changes in brain cholesterol levels in mice treated

with CSL-111 were associated with modest and not significant changes in RNA expression levels of transporters and enzymes involved in cholesterol transport (Supplemental Figure S2).

## **DISCUSSION**

Our data presented herein show that circulating HDL levels affect astrocyte function in the region of the hypothalamus, a brain region important for energy balance. We report for the first time to our knowledge that deficiency of apoA-I results in hypothalamic astrogliosis that is associated with impaired metabolic homeostasis and that administration of rHDL (CSL-111) normalizes hypothalamic inflammation and mitochondrial function. Because our observations were made in mice consuming a chow diet with a very low content of fat (9%), they suggest that low circulating HDL levels directly induce hypothalamic astrocyte dysfunction and metabolic disease, even in the absence of caloric excess. In view of the well-established strong correlation of low HDL and insulin resistance (28), our data imply that individuals with low HDL levels per se have an increased risk for the development of metabolic disease. More importantly, our observations support an emerging paradigm that impairment of HDL function could play a direct role in the pathogenesis of type-2 diabetes.

We observed a marked and specific activation of astrocytes in the absence of apoA-I, with no change in microglial cell status. This is particularly interesting, since it has become increasingly clear that astrocytes, the most abundant glial cell type in the mammalian brain, are critical to essential CNS actions including synaptic transmission, regulation of neural immune responses, antioxidant defense, structural and nutritive support of neurons, and neuronal survival (29). More importantly, recent research has implicated hypothalamic astrocytes as crucial players in the homeostatic control of metabolism by the brain, partly due to their strategic location close to the blood-brain barrier (BBB) (30). Consistent with this, Kim et al. detected an active role of astrocytes in the initiation of hypothalamic synaptic plasticity and neuroendocrine control of feeding by leptin (31). The fact that reactive astrogliosis has been detected in the hypothalamus of high-fat diet-induced obese rodents even before weight gain (5, 31) points to its pivotal role in the pathogenesis of metabolic disease. Our intriguing observation that hypothalamic astrogliosis is enhanced in apoA-I-deficient mice fed a low fat diet and is

associated with the classical signs of metabolic disease may thus provide further evidence for the important role of astrocytes in metabolic control and obesity.

Recent work has indicated that circulating HDLs are important for a well-functioning BBB by promoting cerebrovascular health through several mechanisms. For example, entering the CNS via the choroid plexus (32) HDL may maintain BBB integrity from the luminal side of the vessel by promoting repair of damaged endothelial cells, enhancing endothelial integrity and barrier function. HDL may also prevent deleterious amyloid-beta peptide (A $\beta$ ) accumulation by enhancing its clearance from the brain and accelerating its degradation (33). Consistent with the latter, several investigators have demonstrated *in vitro* that apoA-I inhibits A $\beta$  aggregation into fibrils, and reduces A $\beta$ -induced cytotoxicity, oxidative stress and neuronal degeneration (for review see (34)). Thus there is an increasing effort underway to utilize these beneficial effects of HDLs for the treatment of Alzheimer's disease. For example, it has recently been reported that treatment with HDL-based nanoparticles resulted in decreased A $\beta$  deposition, attenuated reactive gliosis, ameliorated neurological alterations, and reduced memory deficits in an animal model of Alzheimer's disease (35). Most importantly, previous data have shown that apoA-I protects mitochondria by multiple mechanisms involving interaction with CoQ, to stabilize complex II and inhibit ROS-mediated damage to respiratory complexes (14). It seems plausible that these mechanisms may contribute to the herein observed improvement of mitochondrial bioenergetics by administration of HDL particles. In addition, a putative link has been developed in recent years between major players involved in HDL mediated cholesterol reuptake like ABCA1, endocytosis and mitochondrial metabolism (35), but the detailed underlying mechanisms are still unknown. RNA expression data from our study corroborate this link, and ongoing investigations led by us and others are ongoing to fully understand this novel HDL function. Consistent with our observation that HDLs modify mitochondrial bioenergetics in the hypothalamus is the evidence that administration of bezafibrate, a fibrate drug used to lower LDL cholesterol and increase HDL cholesterol levels in the blood, resulted in an increase in mitochondrial proteins and mitochondrial ATP generating capacity (36). Importantly, bezafibrate treatment also attenuated astrogliosis and reduced inflammatory marker levels. Similarly, administration of rHDL (CSL-111) reverses reactive astrogliosis and mitochondrial dysfunction in the hypothalamus of apoA-I<sup>-/-</sup> mice. Collectively, our data reveal that CSL-111

treatment may offer therapeutic potential to correct diet-independent alterations in functional integrity of hypothalamic astrocytes by targeting pathways connecting inflammation and mitochondrial homeostasis.

Our finding that apoA-I directly improves mitochondrial activity in primary astrocytes further supports the hypothesis that HDLs are important in astrocyte function. Although we and others have clearly demonstrated that apoA-I directly modulates metabolism of different cell types within the CNS, it is still unclear how apoA-I-containing lipoprotein particles may exert these direct effects *in vivo* considering that ApoA-I is not produced by glial or neuronal cells within the brain and the BBB may exclude HDL particles from entering from the circulation. It has been hypothesized that apoA-I may be transported from the blood directly across the BBB (for review see 36), and research is ongoing to determine whether pathways similar to its transport in peripheral endothelial cells are involved (37, 38). Even without such a pathway, HDL may be able to reach the cells studied here given the structural differences of the BBB in the hypothalamus and its greater permeability of this barrier to macromolecules (39). The ongoing debate whether ApoA1 proteins cross the BBB is a prominent lack of knowledge due to potential clinical implications, one of them we report herein. Understanding how circulating proteins like apoAI are entering the brain is of pivotal importance for the development of drugs that target specific brain areas important for metabolic control.

Although elevated high-density lipoprotein cholesterol levels in the blood represent one of the strongest epidemiological surrogates for protection against cardiovascular disease (CVD) recent human genetic and pharmacological intervention studies have raised controversy about the causality of this relationship (for review see 40). Collectively all these data indicate that HDL-C concentration in the blood is only giving a static snapshot of a very dynamic and heterogeneous metabolic milieu and is thus unlikely itself causally protective against CVD. It seems more plausible that HDL function is a better predictor of CVD compared to its simple level in the blood, as has been repeatedly shown by several independent groups (41, 42)

In conclusion, our results point to a novel role of HDLs in maintaining normal hypothalamic function.

Circulating HDLs and their major protein component apoA-I have several beneficial functions for brain cell metabolism, including effects on endothelial repair, inflammation, A $\beta$  metabolism and cognitive function, and all of these suggest an HDL-based therapy as a potential treatment for metabolic disease. Since chronic

inflammatory diseases like obesity, type-2 diabetes and cardiovascular disease affect cerebrovascular health (43), it is important to understand whether infusion of HDL particles from healthy subjects may prevent or repair cerebrovascular damage and thus improve metabolic function.

#### **ACKNOWLEDGMENTS/GRANT SUPPORT**

This work was supported by the basic science grant 1-10-BS-72 from the American Diabetes Association, the National Institutes of Health grant 2K12HD051953-06, in part also by the grant from the Deutsche Forschungsgemeinschaft (DFG: SFB1123-A4) and the grant from the Helmholtz Alliance ICEMED-Imaging and Curing Environmental Metabolic Diseases (WP 15) granted to Susanna M. Hofmann.

#### **REFERENCES**

1. Hotamisligil G.S. 2010. Endoplasmic reticulum stress and the inflammatory basis of metabolic disease. *Cell*.140: 900-917.
2. Kälén S., F. L. Heppner, I. Bechmann, M. Prinz, M. H. Tschöp, and C. X. Yi. 2015. Hypothalamic innate immune reaction in obesity. *Nat Rev Endocrinol*.11: 339-51.
3. De Felice F.G. and S. T. Ferreira. 2014. Inflammation, defective insulin signaling, and mitochondrial dysfunction as common molecular denominators connecting type 2 diabetes to Alzheimer disease. *Diabetes*.63: 2262-72.
4. Buckman L.B and K. L. J. Ellacott. 2014. The contribution of hypothalamic macroglia to the regulation of energy homeostasis. *Front Syst Neurosc*.8: 212.
5. Thaler J. P., C. X. Yi, E. A. Schur, S. J. Guyenet, B. H. Hwang, M. O. Dietrich, X. Zhao, D. A. Sarruf, V. Izgur, K. R. Maravilla, H. T. Nguyen, J. D. Fischer, M. E. Matsen, B. E. Wisse, G. J. Morton, T. L. Horvath, D. G. Baskin, M. H. Tschöp, and M. W. Schwartz. 2012. Obesity is associated with hypothalamic injury in rodents and humans. *J Clin Invest*.122: 153-62.

6. Rees K., M. Dyakova, N. Wilson, K. Ward, M. Thorogood, and E. Brunner. 2013. Dietary advice for reducing cardiovascular risk. *Cochrane Database Syst Rev*.12: CD002128.
7. Hooper L., C. D. Summerbell, R. Thompson, D. Sills, F. G. Roberts, H. J. Moore, and G. Davey Smith. 2012. Reduced or modified dietary fat for preventing cardiovascular disease. *Cochrane Database Syst Rev*.5: CD002137.
8. Boden W. E. 2000. High-density lipoprotein cholesterol as an independent risk factor in cardiovascular disease: assessing the data from Framingham to the Veterans Affairs High--Density Lipoprotein Intervention Trial. *Am J Cardiol*.86: 19L-22L.
9. McNeill A. M., K. Katz, C. J. Girman, W. D. Rosamond, L. E. Wagenknecht, J. I. Barzilay, R.P. Tracy, P.J. Savage, and S.A. Jackson. 2006. Metabolic syndrome and cardiovascular disease in older people: The cardiovascular health study. *J Am Geriatr Soc*.54: 1317-24.
10. Stukas S., J. Robert , C. L. Wellington. 2014. High-density lipoproteins and cerebrovascular integrity in Alzheimer's disease. *Cell Metabolism*.19: 574-91.
11. ACCORD Study Group, Ginsberg H. N., M. B. Elam, C. L. Lovato, J. R. Crouse, L. A. Leiter, P. Linz, W. T. Friedewald, J. B. Buse, H. C. Gerstein, J. Probstfield, R. H. Grimm, F. Ismail-Beigi, J. T. Bigger, D. C. Goff, W. C. Cushman, D. G. Simons-Morton, and R.P. Byington. 2010. Effects of combination lipid therapy in type 2 diabetes mellitus. *N Engl J Med*.362: 1563-74.
12. Kingwell B. A., M. J. Chapman, A . Kontush, and N. E. Miller. 2014. HDL-targeted therapies: progress, failures and future. *Nat Rev Drug Discov*.13: 445-64.
13. De Nardo L., L. I. Labzin, H. Kono, R. Seki, S. V. Schmidt, M. Beyer, D. Xu, S. Zimmer, C. Lahrmann , F. A. Schildberg, J. Vogelhuber, M. Kraut, T. Ulas, A. Kerksiek, W. Krebs, N. Bode, A. Grebe, M. L. Fitzgerald, N. J. Hernandez, B. R. G. Williams, P. Knolle, M. Kneilling, M. Röcken, D. Lütjohann , S. D. Wright, J. L. Schultze, and E. Latz .2014. High-density lipoprotein mediates anti-inflammatory reprogramming of macrophages via the transcriptional regulator ATF3. *Nat Immunol*.15: 152-60.
14. . White C. R., G. Datta, and S. Giordano. 2017. High-Density Lipoprotein Regulation of Mitochondrial Function. *Adv Exp Med Biol*.982: 407-429.

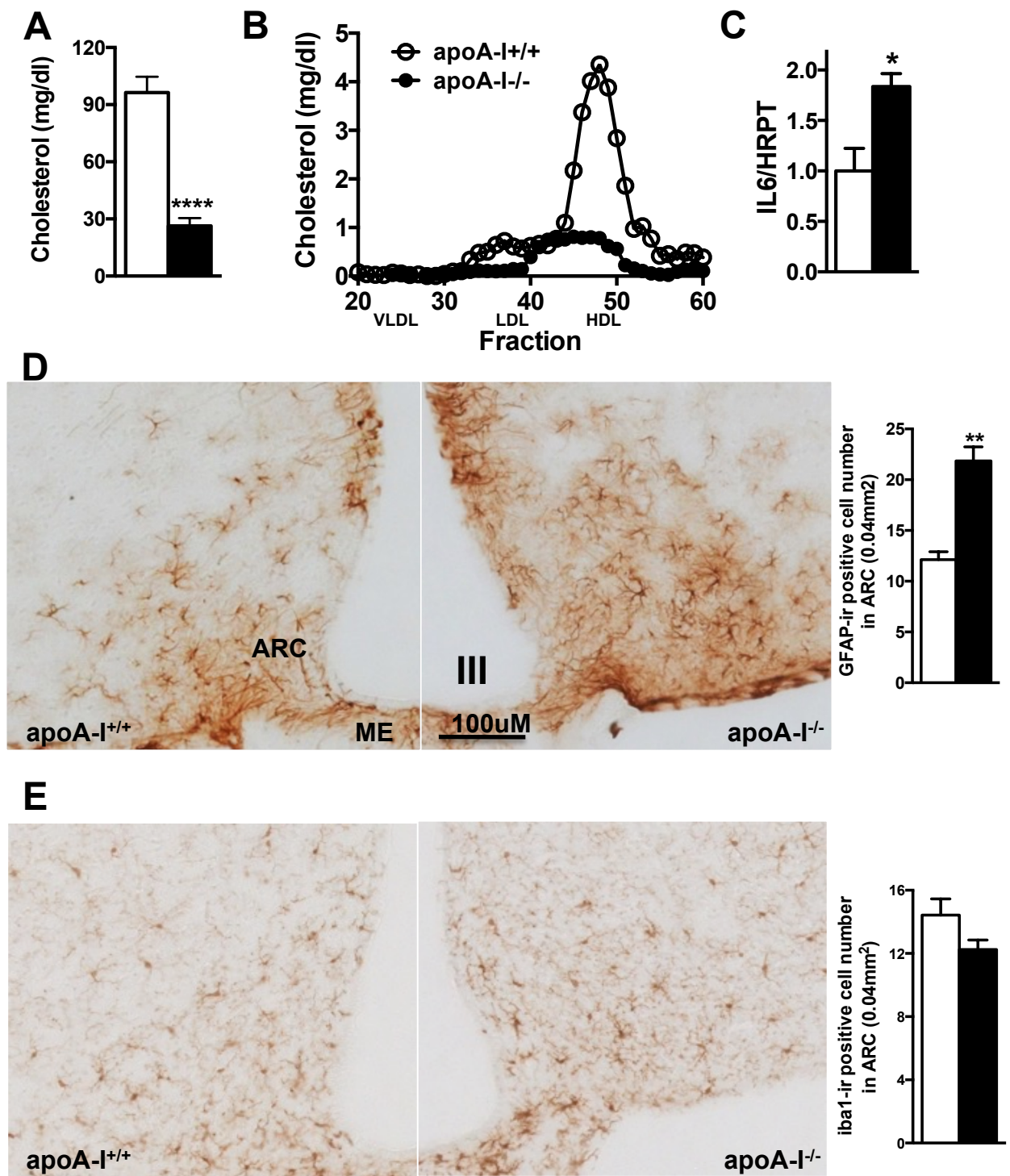
15. Lerch P. G., V. Förtsch, G. Hodler, and R. Bolli. 1996. Production and characterization of a reconstituted high density lipoprotein for therapeutic applications. *Vox Sang.*71: 155-64.
16. Hofmann S. M., L. Zhou, D. Perez-Tilve, T. Greer, E. Grant, L. Wancata, A. Thomas, P. T. Pfluger, J. E. Basford, D. Gilham, J. Herz, M. H. Tschöp, and D. Y. Hui. 2007. Adipocyte LDL receptor-related protein-1 expression modulates postprandial lipid transport and glucose homeostasis in mice. *J Clin Invest.*117: 3271-82.
17. Habegger K. M., D. Matzke, N. Ottaway, J. Hembree, J. Holland, C. Raver, J. Mansfeld, T. D. Müller, D. Perez-Tilve, P. T. Pfluger, S. J. Lee, M. Diaz-Meco, J. Moscat, M. Leitges, M. H. Tschöp, S. M. Hofmann. 2012. Role of adipose and hepatic atypical protein kinase C lambda (PKC $\lambda$ ) in the development of obesity and glucose intolerance. *Adipocyte.*1: 203-2014.
18. Yi C.-X., O. Al-Massadi, E. Donelan, M. Lehti M, J. Weber, C. Ress, C. Trivedi, T. D. Müller, S. C. Woods, and S. M. Hofmann. 2012 Exercise protects against high-fat diet-induced hypothalamic inflammation. *Physiol Behav.*106: 485-90.
19. García-Cáceres C., E. Fuente-Martín, E. Burgos-Ramos, M. Granado, L. M. Frago, V. Barrios, T. Horvath, J. Argente, and J. A. Chowen. 2011. Differential acute and chronic effects of leptin on hypothalamic astrocyte morphology and synaptic protein levels. *Endocrinology.*152: 1809-18.
20. Lehti M., E. Donelan, W. Abplanalp, O. Al-Massadi, K. M. Habegger, J. Weber, C. Ress, J. Mansfeld, S. Somvanshi, C. Trivedi, M. Keuper, T. Ograjsek, C. Striese, S. Cucuruz, P. T. Pfluger, R. Krishna, S. M. Gordon, R. A. Silva, S. Luquet, J. Castel, S. Martinez, D. D'Alessio, W. S. Davidson, and S. M. Hofmann. 2013. High-density lipoprotein maintains skeletal muscle function by modulating cellular respiration in mice. *Circulation.*128: 2364-71.
21. Keuper M., M. Jastroch, C.-X. Yi, P. Fischer-Posovszky, M. Wabitsch, M. H. Tschöp, and S. M. Hofmann. 2014. Spare mitochondrial respiratory capacity permits human adipocytes to maintain ATP homeostasis under hypoglycemic conditions. *FASEB J.*28: 761-70.
22. Brand M. D. 2005. The efficiency and plasticity of mitochondrial energy transduction. *Biochem Soc Trans.*33: 897-904.
23. Mrak R. E., and W. S. T. Griffin. 2005. Glia and their cytokines in progression of neurodegeneration. *Neurobiol Aging.*26: 349-54.

24. Pekny M., and M. Nilsson. 2005. Astrocyte activation and reactive gliosis. *Glia*.50: 427-34.
25. Imai Y., and S. Kohsaka. 2002. Intracellular signaling in M-CSF-induced microglia activation: role of Iba1. *Glia*.40: 164-74.
26. Drake C., H. Boutin, M. S. Jones, A. Denes, B. W. McColl, J. R. Selvarajah, S. Hulme, R. F. Georgiou, R. Hinz, A. Gerhard, A. Vail, C. Prenant, P. Julyan, R. Maroy, G. Brown, A. Smigova, K. Herholz, M. Kassiou, D. Crossman, S. Francis, S. D. Proctor, J. C. Russell, S. J. Hopkins, P. J. Tyrrell, N. J. Rothwell, S. M. Allan. 2011. Brain inflammation is induced by co-morbidities and risk factors for stroke. *Brain Behav Immun*.25: 1113-22.
27. Han R., R. Lai, Q. Ding, Z. Wang, X. Luo, Y. Zhang, G. Cui, J. He, W. Liu, and Y. Chen. 2007. Apolipoprotein A-I stimulates AMP-activated protein kinase and improves glucose metabolism. *Diabetologia*.50: 1960-8.
28. Vollenweider P., A. von Eckardstein, and C. Widmann. HDLs, diabetes, and metabolic syndrome. 2015. *Handb Exp Pharmacol*.224: 405-21.
29. Fuente-Martin E., C. García-Cáceres, E. Morselli, D. J. Clegg, J. A. Chowen, B. Finan, R. D. Brinton, and M. H. Tschöp. 2013. Estrogen, astrocytes and the neuroendocrine control of metabolism. *Rev Endocr Metab Disord*;14: 331-8.
30. García-Cáceres C., C.-X. Yi, and M. H. Tschöp. Hypothalamic astrocytes in obesity. 2013. *Endocrinol Metab Lin North Am*.42: 57-66.
31. Kim J. G., S. Suyama, M. Koch, S. Jin, P. Argente-Arizon, J. Argente, Z. W. Liu, M. R. Zimmer, J. K. Jeong, K. Szigeti-Buck, Y. Gao, C. Garcia-Caceres, C.-Y. Yi, N. Salmaso, F. M. Vaccarino, J. Chowen, S. Diano, M. O. Dietrich, M. H. Tschöp, and T. L. Horvath. 2014. Leptin signaling in astrocytes regulates hypothalamic neuronal circuits and feeding. *Nat Neurosci*.17: 908-10.
32. Horvath T. L., B. Sarman, C. García-Cáceres, P. J. Enriori, P. Sotonyi, M. Shanabrough, E. Borok, J. Argente, J. A. Chowen, D. Perez-Tilve, P. T. Pfluger, H. S. Brönneke, B. E. Levin, S. Diano, M. A. Cowley, and M. H. Tschöp. 2010. Synaptic input organization of the melanocortin system predicts diet-induced hypothalamic reactive gliosis and obesity. *Proc Natl Acad Sci USA*.107: 14875-80.

33. Stukas S., J. Robert, M. Lee, I. Kulic, M. Carr, K. Tourigny, J. Fan, D. Namjoshi, K. Lemke, N. DeValle, J. Chan, T. Wilson, A. Wilkinson, R. Chapanian, J. N. Kizhakkedathu, J. R. Cirrito, M. N. Oda, and G. L. Wellington. 2014. Intravenously injected human apolipoprotein A-I rapidly enters the central nervous system via the choroid plexus. *J Am Heart Assoc.*3: e001156-e.
34. Stukas S., J. Robert, and C. L. Wellington. 2015. High-Density Lipoproteins and Cerebrovascular Integrity in Alzheimer's Disease. *Cell Metabolism.*19: 574-91.
35. Song Q., M. Huang, L. Yao, X. Wang, X. Gu, J. Chen,, J. Huang, Q. Hu,T. Kang, Z. Rong, H. Qi, G. Zheng, H. Chen, and X. Gao. 2014. Lipoprotein-based nanoparticles rescue the memory loss of mice with Alzheimer's disease by accelerating the clearance of amyloid-beta. *ACS nano.*8: 2345-59.
36. Noe N., L. Dillon, V. Lellek, F. Diaz, A. Hida, C. T. Moraes, and T. Wenz. 2013. Bezafibrate improves mitochondrial function in the CNS of a mouse model of mitochondrial encephalopathy. *Mitochondrion.*13:417-26.
37. Cavelier D., P. Ohnsorg, L. Rohrer, and A. von Eckardstein. 2012. The  $\beta$ -chain of cell surface F(0)F(1) ATPase modulates apoA-I and HDL transcytosis through aortic endothelial cells. *Atheroscler Thromb Vasc Biol.*32:131-9.
38. Cavelier D., L. Rohrer, and A. von Eckardstein. ATP-Binding cassette transporter A1 modulates apolipoprotein A-I transcytosis through aortic endothelial cells. 2006. *Circ Res.*99:1060-6.
39. Haddad-Tóvulli R., N. R. V. Dragano, A. F. S. Ramalho, and L. A. Velloso. 2017. Development and Function of the Blood-Brain Barrier in the Context of Metabolic Control. *Front Neurosci.*11: 224.
40. Vitali C., S. A. Khetarpal, D. J. Rader. 2017. HDL Cholesterol Metabolism and the Risk of CHD: New Insights from Human Genetics. *Curr Cardiol Rep.*19: 132.
41. Favari E, M. J Thomas, and M. G. Sorci-Thomas. 2018. High-Density Lipoprotein Functionality as a New Pharmacological Target on Cardiovascular Disease: Unifying Mechanism That Explains High-Density Lipoprotein Protection Toward the Progression of Atherosclerosis. *J Cardiovasc Pharmacol.*71: 325-331.
42. Prillo A., A. L. Catapano, and D. G. Norata. 2018. Biological consequences of dysfunctional HDL. *Curr Med Chem.* May 29.

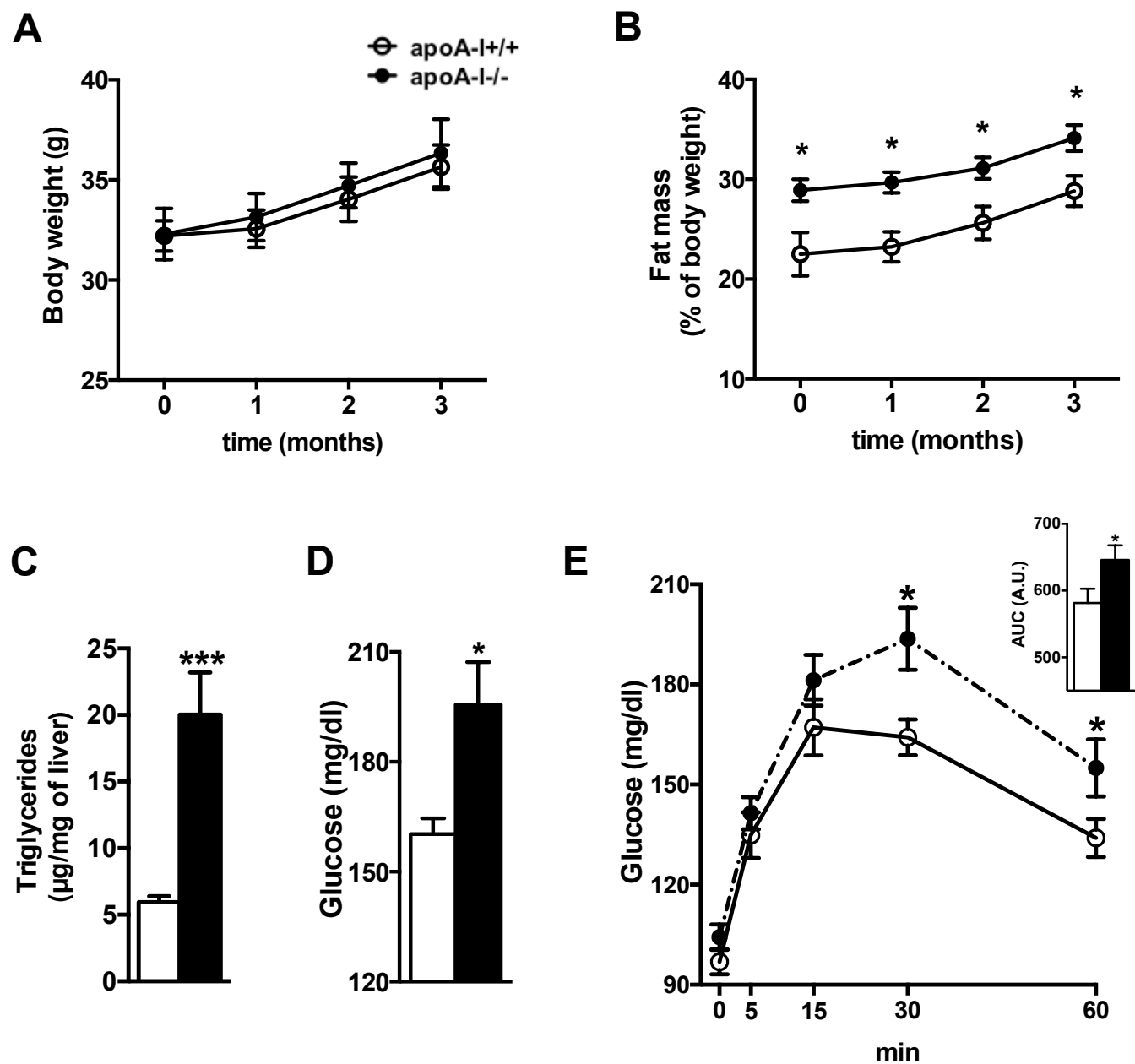
43. Mayeux R., and Y. Stern. Epidemiology of Alzheimer disease. 2012. *Cold Spring Harb Perspect Med.*2: a006239–a.

**Figure 1**

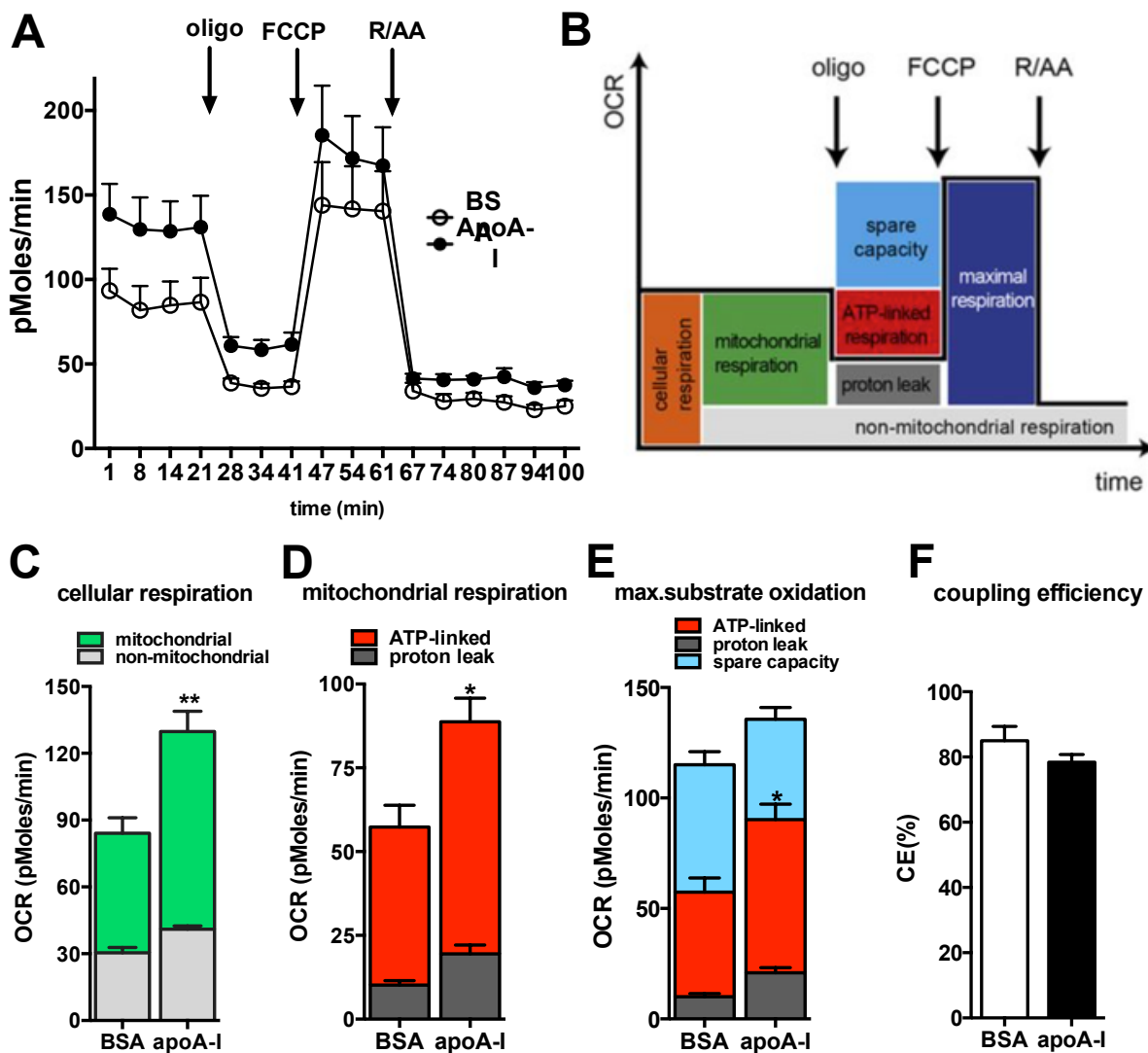


**Figure 1: Reactive astrogliosis is enhanced in the hypothalamic arcuate nucleus of mice with genetically reduced HDL levels.** Total circulating cholesterol levels (A) and HDL particle concentration (B) are markedly reduced in apoA-I-deficient mice (apoA-I<sup>-/-</sup>; closed bars; closed circles) compared to wt mice fed a normal chow diet (apoA-I<sup>+/+</sup>; open bars; open circles) (n=8 mice). IL-6 mRNA levels are significantly increased in hypothalami of apoA-I<sup>-/-</sup> (closed bars) compared to apoA-I<sup>+/+</sup> mice (C). GFAP-immunopositive cells in the ARC of apoA-I deficient mice are significantly increased compared to levels in wt mice (D), but not iba-1 immunopositive cells (E). ARC, arcuate nucleus; ME, median eminence; III: third ventricle. Data are expressed as mean +/- SEM. \*\*P<0.005; \*\*\*\*P<0.00005 vs. wt mice.

**Figure 2**



**Figure 2: Mice with low circulating HDL levels exhibit signs of metabolic disease.** Body composition analysis revealed similar body mass (A), but increased fat mass (B), in apoA-I deficient mice (closed circles) compared to wt littermates (open circles). Liver triglyceride content (C), fasting glucose levels (D) and hepatic glucose output measured by the pyruvate tolerance test (E) were significantly increased in apoA-I-deficient mice (closed bars) compared to levels in wt littermates (open bars). Data are expressed as means +/- SEM. \*P<0.05; \*\*P<0.005; \*\*\*P<0.0005 vs. wt mice.

**Figure 3**

**Figure 3: ApoA-I directly enhances cellular respiration by increasing mitochondrial activity in primary astrocytes.** Cellular respiration and respiration after interference of

mitochondrial pathways with specific inhibitors was analyzed in astrocytes incubated with BSA or apoA-I (20  $\mu$ g/ml overnight) using a XF24 extracellular flux analyzer as described in Materials and Methods. (A) Oxygen consumption rate (OCR) over time in primary astrocytes treated with apoA-I (filled circle) and BSA (open circle). (B) Scheme defining the oxygen-consuming processes of a cell. (C) Cellular respiration was dissected into mitochondrial (green) and non-mitochondrial (gray) respiration using the ETC inhibitors rotenone (R; 25  $\mu$ M) and antimycin A (AA; 25  $\mu$ M). (D) Mitochondrial respiration was further dissected into proton leak (dark gray) and ATP-linked respiration (red) using the ATP-synthase inhibitor oligomycin (oligo; 20  $\mu$ g/ml). (E) Maximal respiration (dark blue) of astrocytes after addition of the chemical uncoupler FCCP (10  $\mu$ M) and after subtracting non-mitochondrial respiration rates. The portion of spare respiratory capacity (light blue) was determined by subtracting basal respiration from maximal respiration rates. (F) Mitochondrial coupling efficiencies were calculated as the fraction of mitochondrial oxygen consumption that is sensitive to oligomycin, reflecting the fraction used to drive ATP synthesis. AU, arbitrary units. All data are expressed as means  $\pm$  SEM of 5 replicates run in parallel. \*P < 0.05, \*\*P < 0.005.

# Figure 4

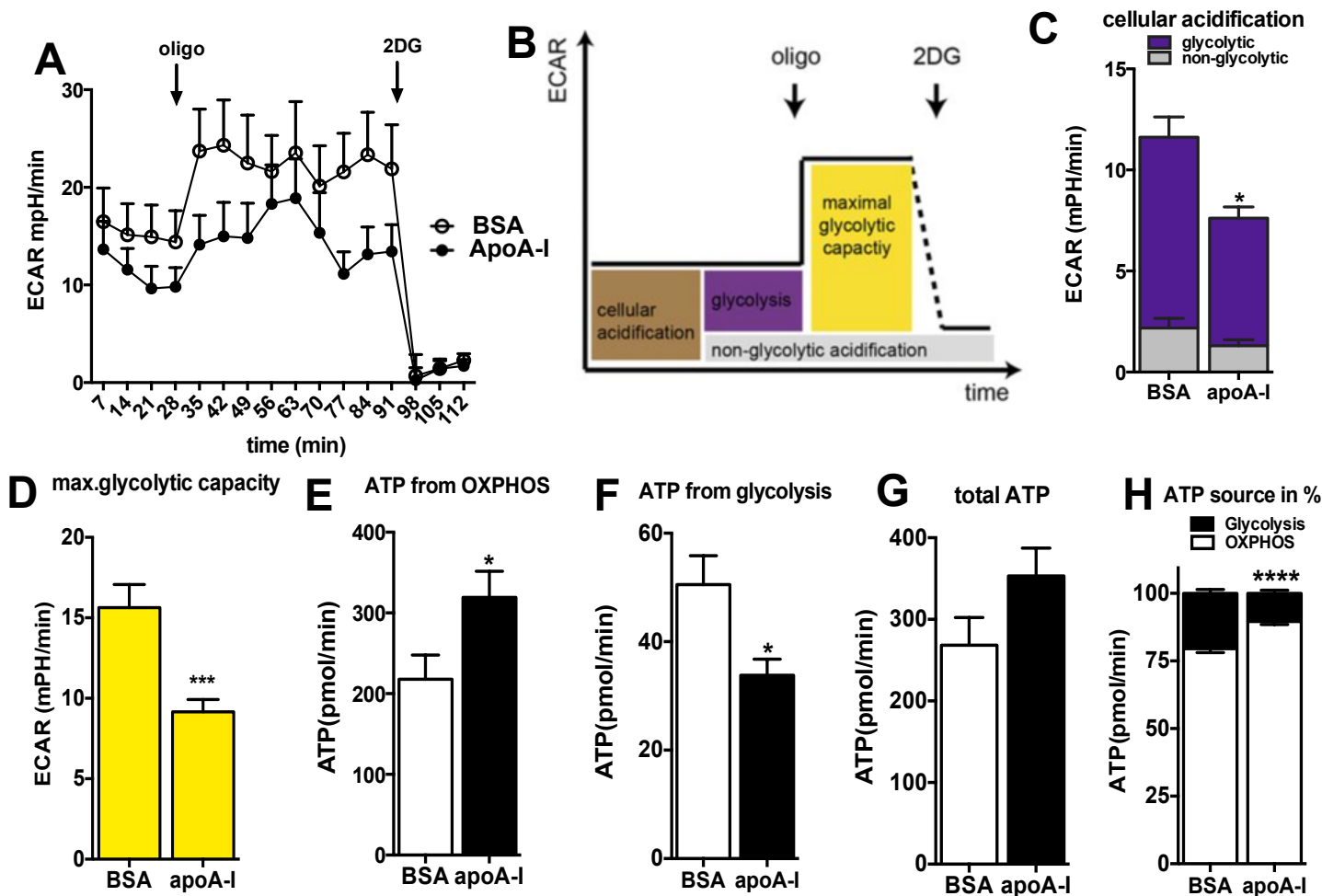


**Figure 4: ApoA-I reduces glycolytic activity in primary astrocytes and enhances ATP demand fueled by oxidative phosphorylation.** (A) Extra-cellular acidification rate (ECAR) was recorded simultaneously with OCR of astrocytes incubated with BSA or apoA-I (20  $\mu\text{g}/\text{ml}$  overnight) with a Seahorse XF96 extracellular flux analyzer, as described in Materials and Methods. (B) Scheme defining cellular ECAR processes. Data after FCCP and rotenone/antimycin A injection were not used for ECAR analysis. (C) By inhibiting glycolysis with 2 deoxy-glucose (2DG; 100 mM) as the last step in the measurements, cellular acidification was broken down to non-glycolytic acidification (gray) and acidification due to glycolysis (purple). (D) By inhibiting mitochondrial ATP synthesis with oligomycin, the maximal glycolytic capacity was obtained. (E) ATP production rates of oxidative phosphorylation pathways of BSA (open bars) and apoA-I (closed bars)-treated primary astrocytes. (F) ATP production rates of glycolysis, as estimated via proton production rates (PPR) of BSA (open bars) and apoA-I (closed bars)-treated primary astrocytes. (G) Sum of ATP produced by oxidative phosphorylation and glycolysis of BSA (open bars) and apoA-I (closed bars)-treated primary astrocytes. (H) Percentage of oxidative phosphorylation (closed bar) and glycolytic (open bar) ATP production on total ATP production in BSA and apoA-I-treated primary astrocytes. Data are expressed as means  $\pm$  SEM of 5 replicates run in parallel. \*P < 0.05, \*\*\*P < 0.0005

# Figure 5

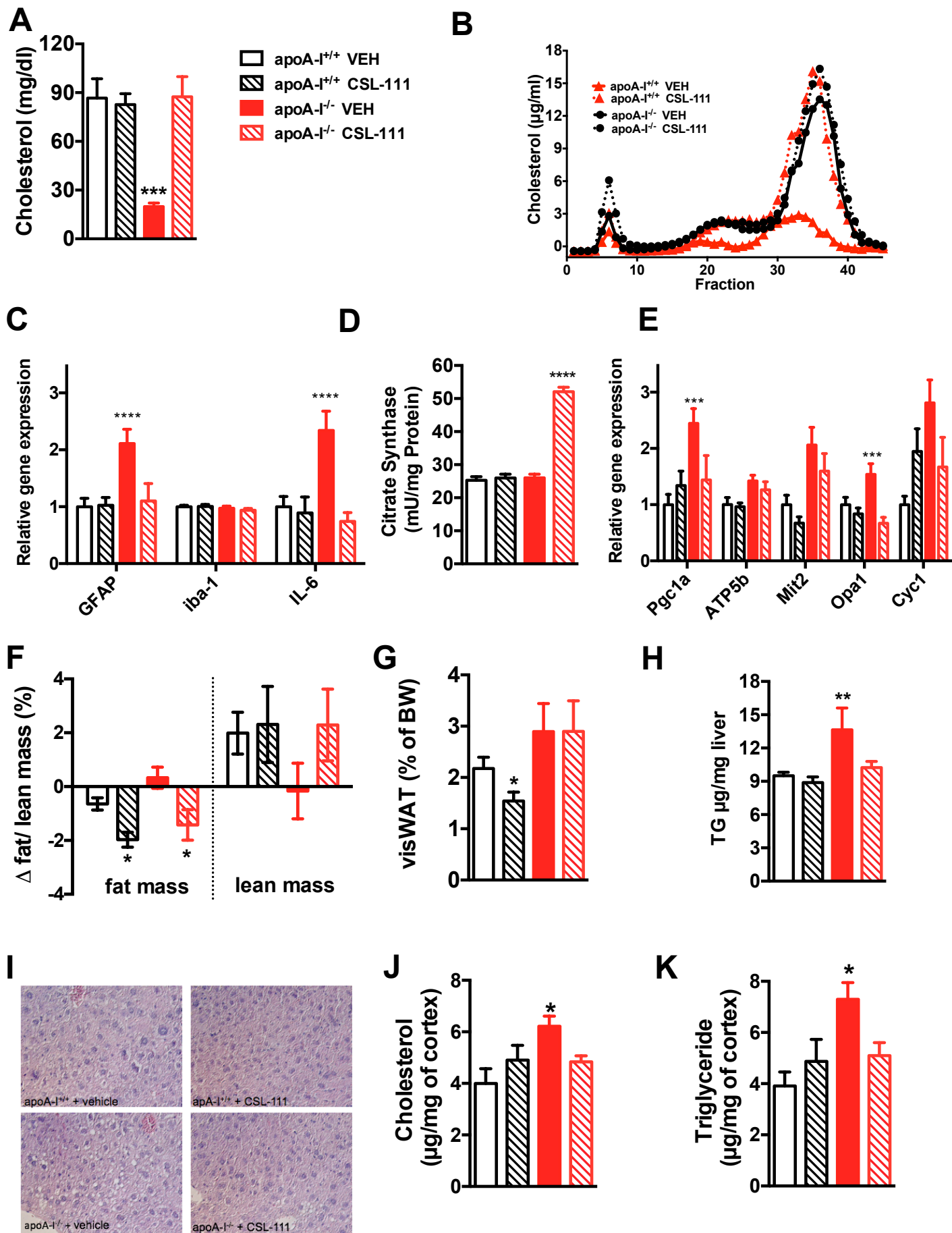


**Figure 5: CSL-111 treatment normalizes hypothalamic inflammation and mitochondrial function markers in chow-fed apoA-I<sup>-/-</sup> mice.** Plasma total cholesterol levels (A) and lipoprotein fractions (B) of apoA-I<sup>+/+</sup> and apoA-I<sup>-/-</sup> mice after daily treatment with CSL-111 at 150mg/kg for 7 days (n=6 mice per group, age 7 months). CSL-111 normalizes hypothalamic inflammation (C) and reverses mitochondrial changes by enhancing citrate synthase activity (D) and normalizing mitochondrial function markers (E) in apoA-I<sup>-/-</sup> mice. Body composition analysis revealed reduced fat mass in apoA-I<sup>+/+</sup> (white hatched bars) and apoA-I<sup>-/-</sup> mice (red hatched bars) treated with CSL-111 compared to vehicle treated groups (F). The changes in body composition were due to reduced visceral fat mass in apoA-I<sup>+/+</sup> mice (white hatched bars) (G) and due to reduced hepatic fat content in apoA-I<sup>-/-</sup> mice (red hatched bars) (H). Representative pictures of H&E-stained hepatic sections from WT and apoA-I<sup>-/-</sup> mice revealed accumulation of hepatic lipids in the form of lipid droplets within the hepatocytes in vehicle treated apoA-I<sup>-/-</sup> mice (40x magnification) which normalized in the CSL-111 treatment group. CSL-111 treatment normalized cholesterol (J) and triglyceride (K) levels in the CNS of apoA-I<sup>-/-</sup> mice. Data are expressed as means ± SEM. \* P<0,05, \*\* P<0,005 vs. apoA-I<sup>+/+</sup> mice.